catalysts

MDPI

Article

Photocatalytic Degradation of Profenofos and Triazophos Residues in the Chinese Cabbage, *Brassica chinensis*, Using Ce-Doped TiO_2

Xiangying Liu [1], You Zhan [1], Zhongqin Zhang [1], Lang Pan [1], Lifeng Hu [1], Kailin Liu [1], Xuguo Zhou [1,2,*] and Lianyang Bai [1,3,*]

1 College of Plant Protection, Hunan Agricultural University, Changsha 410128, China; lxy525525@163.com (X.L.); zyy200023@163.com (Y.Z.); Zhangzhongqin12@163.com (Z.Z.); langpan@hunau.edu.cn (L.P.); zmq525525@163.com (L.H.); zhmy525525@163.com (K.L.)
2 Department of Entomology, University of Kentucky, Lexington, KY 40546-0091, USA
3 Institute of Biotechnology Research, Hunan Academy of Agricultural Sciences, Changsha 410125, China
* Correspondence: xuguozhou@uky.edu (X.Z.); qiyuanzh09@gmail.com (L.B.); Tel.: +1-859-257-3125 (X.Z.); +86-731-8463-5056 (L.B.)

Received: 24 January 2019; Accepted: 15 March 2019; Published: 22 March 2019

Abstract: Pesticides have revolutionized the modern day of agriculture and substantially reduced crop losses. Synthetic pesticides pose a potential risk to the ecosystem and to the non-target organisms due to their persistency and bioaccumulation in the environment. In recent years, a light-mediated advanced oxidation processes (AOPs) has been adopted to resolve pesticide residue issues in the field. Among the current available semiconductors, titanium dioxide (TiO_2) is one of the most promising photocatalysts. In this study, we investigated the photocatalytic degradation of profenofos and triazophos residues in Chinese cabbage, *Brassica chinensis*, using a Cerium-doped nano semiconductor TiO_2 (TiO_2/Ce) under the field conditions. The results showed that the degradation efficiency of these organophosphate pesticides in *B. chinensis* was significantly enhanced in the presence of TiO_2/Ce. Specifically, the reactive oxygen species (ROS) contents were significantly increased in *B. chinensis* with TiO_2/Ce treatment, accelerating the degradation of profenofos and triazophos. Ultra-performance liquid chromatography–mass spectroscopy (UPLC-MS) analysis detected 4-bromo-2-chlorophenol and 1-phenyl-3-hydroxy-1,2,4-triazole, the major photodegradation byproducts of profenofos and triazophos, respectively. To better understand the relationship between photodegradation and the molecular structure of these organophosphate pesticides, we investigated the spatial configuration, the bond length and Mulliken atomic charge using quantum chemistry. Ab initio analysis suggests that the bonds connected by P atom of profenofos/triazophos are the initiation cleavage site for photocatalytic degradation in *B. chinensis*.

Keywords: profenofos; triazophos; photocatalysis; TiO_2/Ce; quantum chemistry

1. Introduction

Profenofos and triazophos are two important organophosphorus pesticides with moderate toxicity, broad spectrum and excellent efficiency. They are widely used on vegetables, cotton, rice and other crops to control insects and mites throughout the world. However, the extensive use of these two compounds, especially the bioaccumulation of their residues, has caused increasing concerns to both human and the environment. For example, it was demonstrated that profenofos and triazophos can induce DNA damage in freshwater fish [1,2]. Traditionally, degradation of pesticide residues is accomplished by physical, chemical, and biological methods [3]. However, physical removal is effective for surface residues. Chemical degradation can lead to the secondary pollution. The secondary

pollutants, such as ozone, ketones and aldehyde compounds, are derived from the degradation of pesticides. Biological degradation can vary greatly due to the ever-changing environmental conditions. Considerable efforts have been invested in the past few years to develop a method that can effectively eliminate pesticide residuals and other organic contaminants in a consistent basis.

Photocatalytic degradation using advanced oxidation processes (AOP) is a promising new approach to deal with the pesticide residues. Excited by photons, it can breakdown pesticides into H_2O, CO_2, and inorganic ions without the secondary pollution. Titanium dioxide (TiO_2) is one of the most investigated semiconductors due to its biological and chemical properties, low cost, negligible toxicity, and high performance [4]. Besides pesticide removal, TiO_2 has also been applied in other fields [5–7], including environmental purification [8,9], food industry [10], health care [11] and agriculture [12]. Although TiO_2 is relatively new to agriculture, it has attracted the attention of an interdisciplinary team of researchers for the sustainable agriculture in the past few years [13]. TiO_2 nanomaterials are most active under the ultraviolet light due to their wide band gap of approximately 3.2 eV [14,15]. Ultraviolet light accounts for approximately 10% of the solar energy [16], it, therefore, limits the application of TiO_2 under the field conditions (e.g., specific intensity and duration of solar illumination, and the physicochemical properties of local soils). To enhance the photocatalytic activity under the visible light, main-group element (Ce, N, C, Ag, etc.) doped nano TiO_2 was extensively applied [17–20]. Among them, Cerium-doped nano TiO_2 (TiO_2/Ce) exhibits a strong photocatalytic capability under the visible lights [20–22]. Liu et al. found TiO_2/Ce can rapidly degrade dimethoate and acephate in vegetables in the field [23,24]. Although dimethoate and acephate are organophosphorus pesticides, they, according to their structures, belong to phosphorodithioate and phosphorothiolamidate, respectively. As a result, dimethoate and acephate have different degradation mechanism and efficiency in the presence of TiO_2/Ce.

In this study, profenofos and triazophos are phosphorothiolate and phosphorothionate organophosphorus pesticides, respectively. Based on our previous knowledge, we hypothesize that TiO_2/Ce will be effective against the residues of profenofos and triazophos; however, the degradation mechanism and efficiency might be different from other organophosphate pesticides used in the vegetable field. To test this hypothesis, we (1) documented the degradation efficiency of TiO_2/Ce against profenofos and triazophos residues in vegetables under the field conditions; (2) identified the photodegradation intermediates of these organophosphate pesticides after TiO_2/Ce treatments; and finally 3) investigated the chemical basis of TiO_2/Ce-mediated photodegradation using molecular structures of these organophosphate pesticides.

2. Results and Discussion

2.1. Degradation Efficiency

Figure 1 shows that the degradation efficiency of profenofos and triazophos increased with time under natural field conditions. At the dosage of 1500 g ai/ha profenofos and 840 g ai/ha triazophos, the degradation efficiency of 34% profenofos and 13% triazophos had been detected in *B. chinensis* after 1 d without TiO_2/Ce. Under the application of TiO_2/Ce at 2400 g ai/ha on the *B. chinensis* leaves, the degradation efficiency of profenofos and triazophos prominently increased. The degradation efficiency of profenofos and triazophos reached 53.3% and 32.1% after 1 d, respectively.

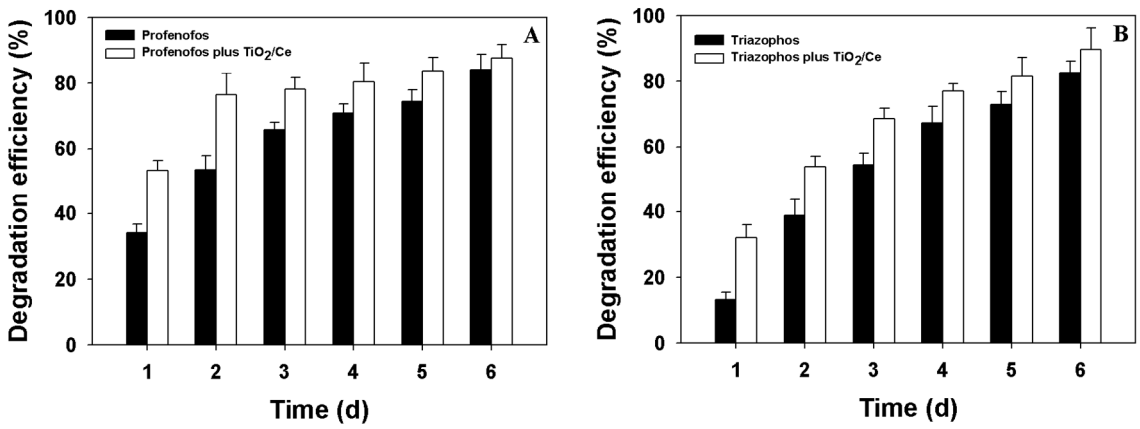

Figure 1. Degradation efficiency of profenofos and triazophos in *B. chinensis*. (**A**) profenofos; (**B**) triazophos.

As a promising material, nano-sized TiO_2 makes a great contribution to sustainable agriculture concerning plant germination and growth [25,26], degradation of pesticides [27], residue detection [28,29], managing diseases and enhancing crop yields [30]. Regarding rapid degradation of organophosphorus pesticides residuals in vegetables using TiO_2 in field conditions, Zeng et al. found that degradation of chlorpyrifos and acephate in tomato leaves increased significantly with rare-earth RE^{3+}-doped nano-TiO_2 [31], and Liu et al. drew a consistent conclusion that the degradation of acephate and dimethoate in Bok choy accelerated remarkably with TiO_2/Ce [23,24]. The results of this study also confirmed that application of TiO_2/Ce improved the degradation of organophosphorus pesticide residues in *B. chinensis* in field trials. The rapid elimination of pesticide residues using multi-doped TiO_2 may be a potential alternative in practical agricultural production. In vegetable production, overuse of organophosphorus pesticides and neglection of the recommended safety interval between pesticide application and harvest often lead to residual amount of pesticide in vegetable exceeding the standards established by the governments. TiO_2/Ce can be applied to targeted vegetables 1–3 d before harvest, which can significantly reduce the pesticide residues and shorten the recommended safety interval. However, the difference of degradation efficiency may be heavily dependent on several factors, including catalyst dosage, pesticide concentration, chemical structures, and pH of the reaction system [23,32].

2.2. Reactive Oxygen Species (ROS) Content and Phytotoxicity

To find the possible cause of the rapid degradation of profenofos and triazophos in the photocatalysis process, reactive oxygen species (ROS) content and phytotoxicity were measured. Figure 2 shows that ROS content in *B. chinensis* treated with TiO_2/Ce was higher than their corresponding untreated controls, suggesting that the application of TiO_2/Ce can increased the ROS contents in *B. chinensis*. One day after treatment, the ROS contents were 5.51 ng/g and 2.00 ng/g in the photocatalysis process of triazophos with and without TiO_2/Ce. Similarly, 5.35 ng/g and 4.15 ng/g in the profenofos photocatalysis process were detected.

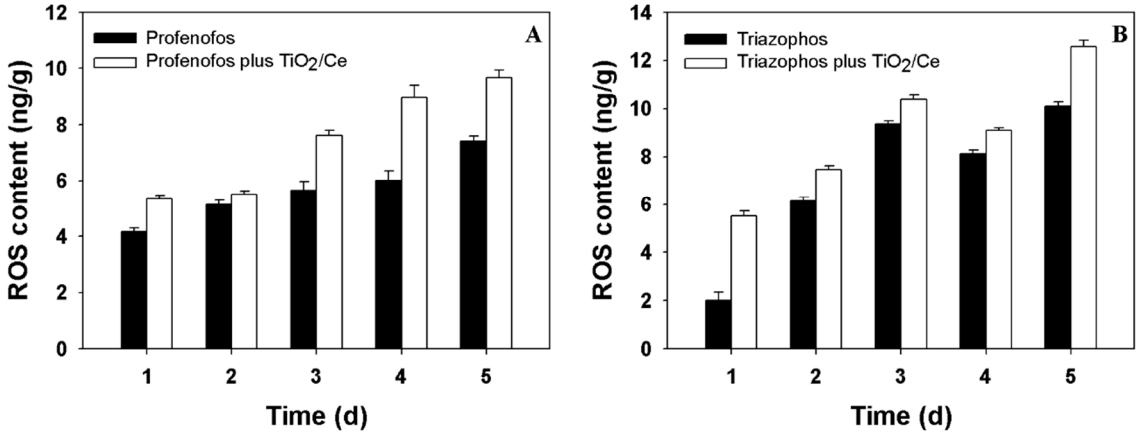

Figure 2. ROS content in *B. chinensis* treated with/without TiO_2/Ce. (**A**) profenofos; (**B**) triazophos.

ROS has strong oxidation characteristics that accelerate the degradation of profenofos and triazophos in Chinese cabbage, *B. chinensis*. However, 4 h after the treatment with TiO_2/Ce hydrosol, some young leaves curled inward, indicating slight phytotoxicity to *B. chinensis* (Figure 3). There are two possible reasons for the plant injury. One major factor is related to ROS content, which dramatically increased under the TiO_2/Ce exposure. Some evidence indicated that the different ROS types have differing abilities to cause cytotoxic properties due to oxidative damage [33–35], which may result in growth inhibition of *B. chinensis*. Another possible factor is associated with the degradation metabolites of profenofos and triazophos, which would be harmful to the growth of vegetables. The phenomenon of pesticide residues and their phytotoxic metabolites was reported by Sirons et al. [36]. However, there was no phytotoxicity during the photocatalytic degradation of dimethoate in bok choy using TiO_2/Ce in the field trials [24]. This inconsistency may be a result of differential degradation products. The injured leaves recovered 24 h after the treatment, and no significant adverse effects were observed in the yield. It merits further investigation whether this slight phytotoxicity of TiO_2/Ce to *B. chinensis* has negative effects on the qualities and nutritions after treatment of food products.

Figure 3. Phytotoxicity symptoms of B. chinensis caused by the application of profenofos/ triazophos with TiO_2/Ce treatment. (**A**) profenofos/triazophos; (**B**) profenofos/triazophos + TiO_2/Ce.

2.3. Degradation Byproducts and Molecular Structure

To investigate the extent of degradation, ultra-performance liquid chromatography–mass spectroscopy (UPLC-MS) analysis was adopted to detect the degradation byproducts generated from the photodegradation reaction system. Figure 4 shows the mass spectrum of profenofos and triazophos and their degradation byproducts. In the analysis of mass spectrum, it was found that the retention times of 5.664, 6.719, 5.156, 4.171 min corresponded with their prominent protonated molecular ions at m/z = 375 $[M + H]^+$, m/z = 230 $[M + Na]^+$, m/z = 314 $[M + H]^+$ and m/z = 178

$[M + H\text{-}NH_3]^+$, respectively, which were identified as profenofos ($C_{11}H_{15}BrClO_3PS$) (Figure 4A), 4-bromo-2-chlorophenol (C_6H_4BrClO) (Figure 4B), triazophos ($C_{12}H_{16}N_3O_3PS$) (Figure 4C) and 1-phenyl-3-hydroxy-1, 2,4-triazole ($C_8H_7N_3O$) (Figure 4D). These compounds were further identified by matching their retention times and mass spectrum with standards under the same UPLC-MS analysis conditions.

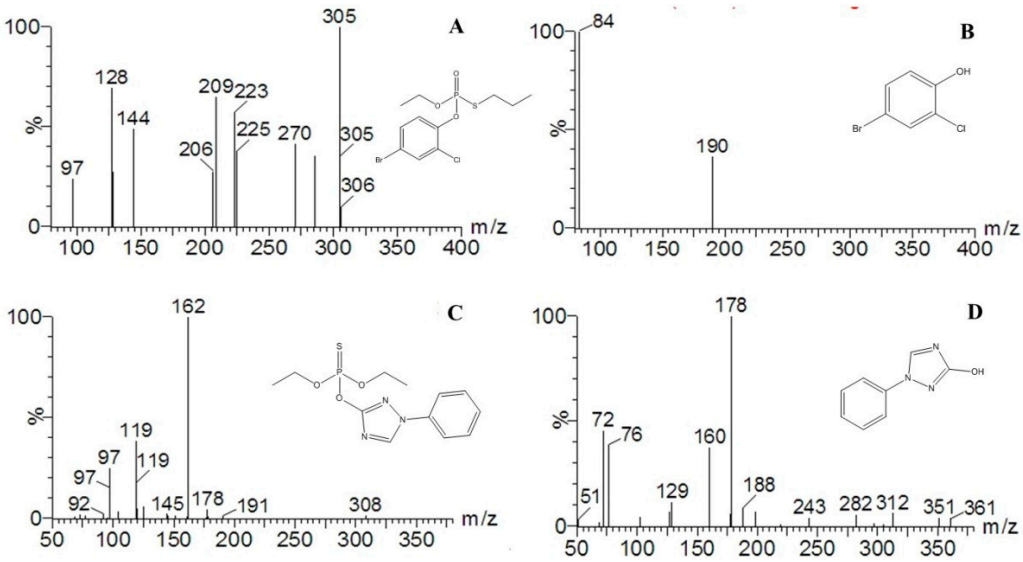

Figure 4. Mass spectra and structures of profenofos, triazophos and their degradation byproducts in *B. chinensis* in the presence of TiO_2/Ce. (**A**) profenofos; (**B**) degradation byproduct of profenofos: 4-bromo-2-chlorophenol; (**C**) triazophos; and (**D**) degradation byproduct of triazophos: 1-phenyl-3-hydroxy-1, 2,4-triazole.

A major metabolic product of profenofos, 4-bromo-2-chlorophenol was widely reported in the photolysis [37], hydrolysis [38], and biodegradation [39,40]. However, there has been no relevant report on photocatalytic degradation products of profenofos using TiO_2. Amalraj et al. [41] Investigated the kinetics of photodegradation of profenofos without focusing on degradation products. Likewise, as a major intermediate of triazophos, 1-phenyl-3-hydroxy-1, 2,4-triazole was identified in the degradation process of photolysis [42], hydrolysis [43,44], and biodegradation [45,46], while 1-phenyl-3-hydroxy-1, 2,4-triazole was detected in the photocatalytic degradation of triazophos in aqueous TiO_2 suspension [47].

According to the structure of profenofos, triazophos, and their metabolites, P-O cleavage of the two targeted pesticides leads to the formation of degradation products 4-bromo-2-chlorophenol and 1-phenyl-3-hydroxy-1, 2,4-triazole, respectively. Bond length and Mulliken atomic charge have been used extensively in quantum chemistry to evaluate the strength of chemical bonds, which is the primary target for pesticide degradation. By calculating the values of bond length and the point charge we can predicte the adsorption sites on TiO_2 particles and the weak position of the molecule in the initial reaction process [48].

To confirm the initial oxidative cleavage site of profenofos and triazophos molecule, bond lengths and Mulliken atomic charges of profenofos and triazophos were calculated based on the optimal geometry conformation of profenofos and triazophos molecules obtained at STO-3G set of Restricted Hartree-Fock (RHF/STO-3) level. The spatial configurations of profenofos and triazophos molecules are shown in Figure 5.

Table 1 shows the bond lengths between main atoms in profenofos and triazophos molecules. In the profenofos molecule, the bond lengths between P^{13}-S^{15}, C^6-Br^{10}, C^2-Cl^{11}, P^{13}-O^{26} and P^{13}-O^{12} are 2.1100×10^{-10}, 1.91000×10^{-10}, 1.78000×10^{-10}, 1.76000×10^{-10}, 1.76000×10^{-10}, and 1.76000×10^{-10} m, respectively, which are longer than other bonds. Similarly, the bond lengths

between P^{19}-S^{20} in the triazophos molecule is the longest with the value of 1.85680×10^{-10} m, followed by the bond lengths between P^{19}-O^{18}, P^{19}-O^{21} and P^{19}-O^{22} with the same value of 1.76000×10^{-10} m. According to negative correlation between bond energy and bond length [49], the above longer bonds tend to cleave when attacked by ROS. This means the P^{13}-O^{12} bond in the profenofos molecule and the P^{19}-O^{18} bond in triazophos molecules are attacked first, leading to the P^{13}-O^{12} bond cleavage in profenofos and generating its intermediate product 4-bromo-2-chlorophenol. Likewise, the P^{19}-O^{18} bond in triazophos molecules is easier to cleave and generates the degradation metabolite 1-phenyl-3-hydroxy-1, 2,4-triazole.

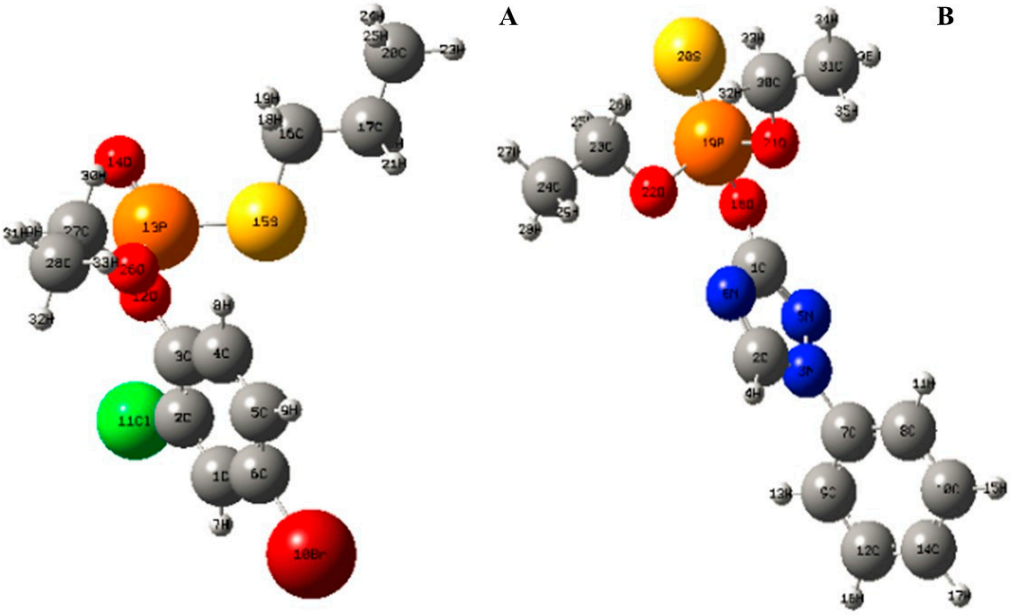

Figure 5. Spatial configuration of profenofos and triazophos molecule. (**A**) profenofos; (**B**) triazophos.

Table 1. Bond length on main atoms in profenofos or triazophos molecules.

Pesticide	Bond	Bond Length ($\times 10^{-10}$ m)	Bond	Bond Length ($\times 10^{-10}$ m)
Profenofos	P^{13}-O^{14}	1.45200	C^{16}-C^{17}	1.50715
	P^{13}-O^{26}	1.76000	C^{17}-C20	1.50713
	P^{13}-O^{12}	1.76000	O^{26}-C^{27}	1.43000
	P^{13}-S^{15}	2.11000	C^{27}-C^{28}	1.50025
	C^{16}-S^{15}	1.78000	O^{12}-C^{3}	1.43000
	C^{3}-C^{4}	1.39543	C^{1}-C^{2}	1.39516
	C^{4}-C^{5}	1.39483	C^{2}-Cl^{11}	1.76000
	C^{5}-C^{6}	1.39514	C^{2}-C^{3}	1.39471
	C^{6}-Br^{10}	1.91000	C^{6}-C^{1}	1.39483
Triazophos	P^{19}-S^{20}	1.85680	N^{3}-C^{7}	1.47000
	P^{19}-O^{18}	1.76000	C^{7}-C^{8}	1.39516
	P^{19}-O^{21}	1.76000	C^{7}-C^{9}	1.39483
	P^{19}-O^{22}	1.76000	C^{8}-C^{10}	1.39471
	O^{18}-C^{1}	1.43000	C^{9}-C^{12}	1.39514
	C^{1}-N^{5}	1.40175	C^{10}-C^{14}	1.39543
	C^{1}-N^{6}	1.43487	C^{12}-C^{14}	1.39483
	C^{2}-N^{6}	1.40185	O^{21}-C^{30}	1.43000
	C^{2}-N^{3}	1.39180	O^{22}-C^{23}	1.43000
	N^{3}-N^{5}	1.39180	C^{30}-C^{31}	1.50025
	C^{23}-C^{24}	1.50025		

Based on the Mulliken atomic charges of profenofos and triazophos (Table 2), the P^{13} atom is located at the profenofos molecule, and the P^{19} atom is located at the triazophos molecule. They are the largest positive point charges, with values 1.020008 and 1.018974, respectively, suggesting that the P^{13} atom in the profenofos molecule and the P^{19} atom in the triazophos molecule are the most likely to be attacked by nucleophilic reagents such as H_2O and OH^-. This also demonstrates the bonds between atoms connected with phosphorus atom are the vulnerable site in the profenofos and triazophos molecule. Therefore, the P^{13}-S^{15}, C^6-Br^{10}, C^2-Cl^{11}, P^{13}-O^{26}, P^{13}-O^{12} bond in the profenofos molecule and P^{19}-S^{20}, P^{19}-O^{18}, P^{19}-O^{21} and P^{19}-O^{22} bond in the triazophos molecule are weaker sites under attack, which is in accordance with the results of bond length. This demonstrates that the P^{13} in the profenofos molecule and the P^{19} bond in the triazophos molecule are the possible degradation initiation sites of profenofos and triazophos.

Table 2. Mulliken atomic charges of profenofos and triazophos molecule.

Pesticide	Atom	Charge	Atom	Charge
Profenofos	C^1	−0.050417	P^{13}	1.020008
	C^2	0.035499	O^{14}	−0.505145
	C^3	0.114263	S^{15}	0.021148
	C^4	−0.084254	C^{16}	−0.191632
	C^5	−0.050410	C^{17}	−0.096471
	C^6	−0.049715	C^{20}	−0.177921
	Br^{10}	0.015273	O^{26}	−0.381770
	Cl^{11}	−0.139687	C^{27}	0.000156
	O^{12}	−0.363450	C^{28}	−0.180574
Triazophos	C^1	0.249223	C^{14}	−0.06174
	C^2	0.138768	O^{18}	−0.35249
	N^3	−0.17545	P^{19}	1.018974
	N^5	−0.16349	S^{20}	−0.33818
	N^6	−0.27804	O^{21}	−0.36477
	C^7	0.116977	O^{22}	−0.36329
	C^8	−0.07132	C^{23}	0.002962
	C^9	−0.06147	C^{24}	−0.17913
	C^{10}	−0.05342	C^{30}	0.00403
	C^{12}	−0.0536	C^{31}	−0.17975

In addition, there is a phosphoester bond in the profenofos molecular structure and a phosphorothioate ester bond in the triazophos molecular structure. The hydrolysis of ester bonds can lead to the generation of 4-bromo-2-chlorophenol and 1-phenyl-3-hydroxy-1, 2,4-triazole, respectively. This metabolic process was confirmed in the degradation of profenofos in melon [50] and of triazophos in paddy soil [43]. This is a common metabolic process during the decomposition of organophosphorus pesticides [51]. However, hydrolysis is the reaction related to the substitution reaction of a nucleophilic group, and it is relatively slow and impractical to treat the pesticide residues in the field conditions. Photocatalytic degradation is a process of the chemical bond cleavage of molecules associated with the pesticide molecular and other quantum parameters (e.g., bond length, atomic charges). TiO_2 -based photocatalysis was a rapid and efficient degradation. It simultaneously is able to completely mineralize the atom carbon (C), hydrogen (H), sulfur (S) and nitrogen (N) in the pesticide molecular into CO_2, H_2O, into SO_4^{2-}, NO_3^- ions [52]. Further work is needed to confirm whether TiO_2 -based photocatalysis and hydrolysis may coexist in the degradation of profenofos and triazophos.

3. Materials and Methods

3.1. Materials

Seeds of the Chinese cabbage, *Brassica chinensis*, were brought from Guilin Huifeng Seed Co., Ltd. (Guangxi province, China). Nano TiO_2/Ce (0.6% hydrosol, the average particle size of 10 nm, and the absorption onset of 455 nm) was obtained from the Panzhihua Iron & Steel Group Co. (Sichuan province, China). Standards of profenofos (95% purity) and triazophos (70% purity) were bought from Dr. Ehrenstorfer (Augsburg, Germany). The formulations of profenofos (50% emulsifiable concentrate, EC) and triazophos (20% EC) were purchased from local vendors of Jiangsu Futian Co., Ltd. (Jiangsu province, China) and Xiangtan Shaoshan Co., Ltd. (Hunan province, China), respectively. Enzyme-linked immunoassay (ELISA) Kit of plant ROS was purchased from Tsz Biosciences (San Francisco, CA, USA). Methanol and acetone (chromatographical grade) were purchased from Tedia Company Inc. (Fairfield, OH, USA).

3.2. Sample Preparation

Photodegradation of profenofos and triazophos using TiO_2/Ce was carried out at the research station of Hunan Agricultural University. All field trials were strictly followed the Guideline on Pesticide Residue Trials (NY/T 788-2004) issued by the Ministry of Agriculture, People's Republic of China. According to the guideline, it is not necessary to reapply pesticides or take into account of dew's effect during the pesticide residue trial if no rainfall occurs within the first two hours of pesticide application in the field. The pesticide dosage is calculated by the plot area, not by the foliage area. In this study, the impact of environmental factors (e.g., the amount of sunlight) was the same for both control and TiO_2/Ce treatment because all experiments were carried out within the same vegetable plot in a randomized design. That been said, the uncontrollable nature of the enviromental factors could, potentially, impact the outcome of this research. *Brassica chinensis* seeds were directly sowed in the field. After 25 d of growth, *B. chinensis* were sprayed with 50% profenofos EC at 1500 g ai/ha and 20% triazophos EC at 846 g ai/ha, a 2*X* recommended dosage in the field to facilitate the detection of degradation products. After 2 h of pesticide application, TiO_2/Ce hydrosol was sprayed to the same *B. chinensis* plant at 2400 g ai/ha, the optimum concentration of TiO_2/Ce on organophosphorus pesticides degradation [23,24]. Pesticide-treated *B. chinensis*, without TiO_2/Ce hydrosol application, was used as the control. After 0, 1, 2, 3, 4, 5, and 6 d, *B. chinensis* were collected using a 5-point sampling approach. The extraction, concentration, purification of profenofos, triazophos and their degradation products in *B. chinensis* were followed Liu et al. [24]. Specifically, 20 g of shredded *B. chinensis* samples, 50 mL of acetonitrile, and 5 g of sodium chloride were placed into a glass centrifuge tube for 3-min homogenization at 15,000 rpm/min, and then centrifuged for 5 min at 5000 rpm/min. The resultant 10 mL of supernatants were purified by the solid phase extraction (SPE) column. The eluents were concentrated to dryness by a rotary evaporator at 40 °C, and the residues were dissolved, respectively, in 2 mL acetone for GC analysis and 2 mL methanol for UPLC-MS analysis.

3.3. GC analysis

To assess the photocatalytic degradation efficiency, the amount of profenofos and triazophos residue in *B. chinensis* was determined by GC-2010 (Shimadzu, Kyoto, Japan). The GC analysis conditions of profenofos and triazophos are shown in Table 3.

Table 3. Gas chromatography analysis conditions.

Analysis Conditions	Profenofos	Triazophos
Injector temperature	250 °C	220 °C
Detector temperature	Electron capture detector (ECD) 330 °C	Flame photometric detector (FPD) 250 °C
Injection volume	1 μL	1 μL
Split ratio	5	5
Carrier gas	Nitrogen	Nitrogen
Separation column	RTX-5 capillary column (30 m × 0.25 mm × 0.25 μm)	RTX-5 capillary column (30 m × 0.25 mm × 0.25 μm)
Column volume	1.5 mL/min	1.5 mL/min
Column temperature	Programmed at 150 °C, kept for 1 min, then increased from 150 °C to 240 °C at 10 °C/min, and kept at 240 °C for 5 min.	Programmed at 120 °C, kept for 1 min, next increased from 120 °C to 200 °C at 20 °C/min, kept for 6 min, then from 200 °C to 240 °C at 20 °C/min, and kept at 240 °C for 6 min.

3.4. ROS Assay

To determine the possible cause of the rapid degradation of profenofos and triazophos in the presence of TiO_2/Ce, ROS content in *B. chinensis* was measured after 1, 2, 3, 4 and 5 d of TiO_2/Ce application. The ROS content was measured using ELISA method described by Liu et al. [24] in combination with the instructions of the ELISA Kit of plant ROS.

3.5. UPLC-MS Analysis

B. chinensis samples were collected for UPLC-MS analysis 1 d after TiO_2/Ce application. The degradation products of profenofos and triazophos in Chinese cabbage were detected using UPLC-MS (Waters Corp, Milford, MA, USA). UPLC-MS analysis conditions were set by Liu et al. [24]. The data from UPLC-MS detection abundance were analyzed using MassLynx V4.1 software (Waters Corp., Milford, MA, USA).

3.6. RHF/STO-3G Calculation

At first, the optimal spatial geometry conformations of profenofos and triazophos molecule were predicted at STO-3G set of Restricted Hartree-Fock (RHF/STO-3G) of the software GaussView 3.08. Then, the bond length and the Mulliken atomic of profenofos and triazophos molecule were calculated.

3.7. Data Analysis

There were three replications for each treatment in all experiments. The degradation efficiency was calculated using the equation: $\eta = (P_t - P_0)/P_0 \times 100\%$, where η is the degradation efficiency of profenofos or triazophos, P_0 and P_t denotes the amount of profenofos or triazophos in *B. chinensis* before TiO_2/Ce hydrosol treatment and after application of TiO_2/Ce for t days, respectively.

4. Conclusions

The photocatalytic degradation of profenofos and triazophos in *B. chinensis* has been studied by TiO_2/Ce hydrosol under the field conditions. The degradation rate of profenofos and triazophos were much faster with TiO_2/Ce than that of direct natural degradation. One of the reasons for the rapid degradation was the increase ROS generated by TiO_2/Ce. Degradation products were identified as 4-bromo-2-chlorophenol from profenofos and 1-phenyl-3-hydroxy-1, 2,4-triazole from triazophos, confirmed by quantum chemistry analyses. Photocatalytic degradation of profenofos or triazophos shows great promise as an effective semiconductor to remove pesticide residues in vegetables.

Author Contributions: Conceptualization, X.L. and X.Z.; Data curation, L.H.; Formal analysis, Y.Z.; Funding acquisition, X.L.; Investigation, Z.Z. and K.L.; Project administration, L.B.; Supervision, X.Z.; Validation, X.Z.; Writing—original draft, X.L.; Writing—review & editing, L.P. and X.Z.

Funding: This research was funded by the National Natural Science Foundation of China (grant number 31672043 and 21003042), the Natural Science Foundation of Hunan Province (grant number 2018JJ2165), China Postdoctoral Science Foundation funded project (grant number 2015M582329), and China Scholarship Council (grant number 201608430210).

Acknowledgments: We are grateful to anonymous reviewers for their constructive comments. We thank Mingxing He for providing TiO_2/Ce.

Conflicts of Interest: The authors have declared that no conflict of interest exists.

References

1. Ghaffar, A.; Hussain, R.; Khan, A.; Rao, Z.A. Hemato-biochemical and Genetic Damage Caused by Triazophos in Fresh Water Fish, *Labeo rohita*. *Int. J. Agric. Biol.* **2015**, *17*, 637–642. [CrossRef]
2. Pandey, A.K.; Nagpure, N.; Trivedi, S.P.; Kumar, R.; Kushwaha, B. Profenofos induced DNA damage in freshwater fish, Channa punctatus (Bloch) using alkaline single cell gel electrophoresis. *Mutat. Res.-Gen. Toxicol. Environ. Mutagenesis* **2011**, *726*, 209–214. [CrossRef] [PubMed]
3. Bajwa, U.; Sandhu, K.S. Effect of handling and processing on pesticide residues in food—A review. *J. Food Sci. Technol.* **2014**, *51*, 201–220. [CrossRef]
4. Carp, O.; Huisman, C.L.; Reller, A. Photoinduced reactivity of titanium dioxide. *Prog. Solid State Chem.* **2004**, *32*, 33–177. [CrossRef]
5. He, Y.; Sutton, N.B.; Rijnaarts, H.H.; Langenhoff, A.A. Degradation of pharmaceuticals in wastewater using immobilized TiO_2 photocatalysis under simulated solar irradiation. *Appl. Catal. B-Environ.* **2016**, *182*, 132–141. [CrossRef]
6. Khavar, A.H.C.; Moussavi, G.; Mahjoub, A.R.; Satari, M.; Abdolmaleki, P. Synthesis and visible-light photocatalytic activity of In, S-TiO_2@rGO nanocomposite for degradation and detoxification of pesticide atrazine in water. *Chem. Eng. J.* **2018**, *345*, 300–311. [CrossRef]
7. Lu, P.-J.; Huang, S.-C.; Chen, Y.-P.; Chiueh, L.-C.; Shih, D.Y.-C. Analysis of titanium dioxide and zinc oxide nanoparticles in cosmetics. *J. Food Drug Anal.* **2015**, *23*, 587–594. [CrossRef] [PubMed]
8. Isaifan, R.J.; Samara, A.; Suwaileh, W.; Johnson, D.; Yiming, W.; Abdallah, A.A.; Aïssa, B. Improved self-cleaning properties of an efficient and easy to scale up TiO_2 thin films prepared by adsorptive self-assembly. *Sci. Rep.-UK* **2017**, *7*, 9466. [CrossRef] [PubMed]
9. Yang, C.; Zhang, M.; Dong, W.; Cui, G.; Ren, Z.; Wang, W. Highly efficient photocatalytic degradation of methylene blue by PoPD/TiO_2 nanocomposite. *PLoS ONE* **2017**, *12*, e0174104. [CrossRef]
10. Kumari, A.; Yadav, S.K. Nanotechnology in agri-food sector. *Crit. Rev. Food Sci.* **2014**, *54*, 975–984. [CrossRef]
11. Koklic, T.; Urbancic, I.; Zdovc, I.; Golob, M.; Umek, P.; Arsov, Z.; Drazic, G.; Pintaric, S.; Dobeic, M.; Strancar, J. Surface deposited one-dimensional copper-doped TiO_2 nanomaterials for prevention of health care acquired infections. *PLoS ONE* **2018**, *13*, e0201490. [CrossRef] [PubMed]
12. Wang, Y.; Sun, C.; Zhao, X.; Cui, B.; Zeng, Z.; Wang, A.; Liu, G.; Cui, H. The application of nano-TiO_2 photo semiconductors in agriculture. *Nanoscale Res. Lett.* **2016**, *11*, 529. [CrossRef] [PubMed]
13. Prasad, R.; Kumar, V.; Prasad, K.S. Nanotechnology in sustainable agriculture: Present concerns and future aspects. *Afr. J. Biotechnol.* **2014**, *13*, 705–713.
14. Gogos, A.; Knauer, K.; Bucheli, T.D. Nanomaterials in plant protection and fertilization: Current state, foreseen applications, and research priorities. *J. Agric. Food Chem.* **2012**, *60*, 9781–9792. [CrossRef] [PubMed]
15. Kumar, S.G.; Devi, L.G. Review on modified TiO_2 photocatalysis under UV/visible light: Selected results and related mechanisms on interfacial charge carrier transfer dynamics. *J. Phys. Chem. A* **2011**, *115*, 13211–13241. [CrossRef] [PubMed]
16. Chen, X.; Mao, S.S. Titanium dioxide nanomaterials: Synthesis, properties, modifications, and applications. *Chem. Rev.* **2007**, *107*, 2891–2959. [CrossRef]
17. Xie, C.; Yang, S.; Shi, J.; Niu, C. Highly crystallized C-doped mesoporous anatase TiO_2 with visible light photocatalytic activity. *Catalysts* **2016**, *6*, 117. [CrossRef]

18. Kamaei, M.; Rashedi, H.; Dastgheib, S.; Tasharrofi, S. Comparing photocatalytic degradation of gaseous ethylbenzene using N-doped and pure TiO_2 nano-catalysts coated on glass beads under both UV and visible light irradiation. *Catalysts* **2018**, *8*, 466. [CrossRef]
19. Lin, Y.; Mehrvar, M. Photocatalytic treatment of an actual confectionery wastewater using $Ag/TiO_2/Fe_2O_3$: Optimization of photocatalytic reactions using surface response methodology. *Catalysts* **2018**, *8*, 409. [CrossRef]
20. Mikaeili, F.; Topcu, S.; Jodhani, G.; Gouma, P.-I. Flame-sprayed pure and Ce-doped TiO_2 photocatalysts. *Catalysts* **2018**, *8*, 342. [CrossRef]
21. Charanpahari, A.; Umare, S.; Sasikala, R. Effect of Ce, N and S multi-doping on the photocatalytic activity of TiO_2. *Appl. Surf. Sci.* **2013**, *282*, 408–414. [CrossRef]
22. Xie, J.; Jiang, D.; Chen, M.; Li, D.; Zhu, J.; Lü, X.; Yan, C. Preparation and characterization of monodisperse Ce-doped TiO_2 microspheres with visible light photocatalytic activity. *Colloid Surf. A* **2010**, *372*, 107–114. [CrossRef]
23. Liu, X.; Wang, L.; Zhou, X.; Liu, K.; Bai, L.; Zhou, X. Photocatalytic degradation of acephate in pak choi, Brassica chinensis, with Ce-doped TiO_2. *J. Environ. Sci. Health B.* **2015**, *50*, 331–337. [CrossRef] [PubMed]
24. Liu, X.; Li, Y.; Zhou, X.; Luo, K.; Hu, L.; Liu, K.; Bai, L. Photocatalytic degradation of dimethoate in Bok choy using cerium-doped nano titanium dioxide. *PLoS ONE* **2018**, *13*, e0197560. [CrossRef] [PubMed]
25. Feizi, H.; Rezvani Moghaddam, P.; Shahtahmassebi, N.; Fotovat, A. Impact of bulk and nanosized titanium dioxide (TiO_2) on wheat seed germination and seedling growth. *Biol. Trace Elem. Res.* **2012**, *146*, 101–106. [CrossRef] [PubMed]
26. Zheng, L.; Hong, F.; Lu, S.; Liu, C. Effect of nano-TiO_2 on strength of naturally aged seeds and growth of spinach. *Biol. Trace Elem. Res.* **2005**, *104*, 83–91. [CrossRef]
27. Affam, A.C.; Chaudhuri, M. Degradation of pesticides chlorpyrifos, cypermethrin and chlorothalonil in aqueous solution by TiO_2 photocatalysis. *J. Environ. Manag.* **2013**, *130*, 160–165. [CrossRef] [PubMed]
28. Huang, Y.; Zhou, Q.; Xie, G.; Liu, H.; Lin, H. Titanium dioxide nanotubes for solid phase extraction of benzoylurea insecticides in environmental water samples, and determination by high performance liquid chromatography with UV detection. *Microch. Acta* **2011**, *172*, 109–115. [CrossRef]
29. Geng, H.R.; Miao, S.S.; Jin, S.F.; Yang, H. A newly developed molecularly imprinted polymer on the surface of TiO_2 for selective extraction of triazine herbicides residues in maize, water, and soil. *Anal. Bioanal. Chem.* **2015**, *407*, 8803–8812. [CrossRef] [PubMed]
30. Owolade, O.; Ogunleti, D. Effects of titanium dioxide on the diseases, development and yield of edible cowpea. *J. Plant Prot. Res.* **2008**, *48*, 329–336. [CrossRef]
31. Zeng, R.; Wang, J.; Cui, J.; Hu, L.; Mu, K. Photocatalytic degradation of pesticide residues with RE^{3+}-doped nano-TiO_2. *J. Rare Earths* **2010**, *28*, 353–356. [CrossRef]
32. Rabindranathan, S.; Devipriya, S.; Yesodharan, S. Photocatalytic degradation of phosphamidon on semiconductor oxides. *J. Hazard. Mater.* **2003**, *102*, 217–229. [CrossRef]
33. Apel, K.; Hirt, H. Reactive oxygen species: Metabolism, oxidative stress, and signal transduction. *Annu. Rev. Plant Biol.* **2004**, *55*, 373–399. [CrossRef] [PubMed]
34. Zhang, S.; Qiu, C.B.; Zhou, Y.; Jin, Z.P.; Yang, H. Bioaccumulation and degradation of pesticide fluroxypyr are associated with toxic tolerance in green alga Chlamydomonas reinhardtii. *Ecotoxicology* **2011**, *20*, 337–347. [CrossRef] [PubMed]
35. Yan, Z.-Q.; Wang, D.-D.; Ding, L.; Cui, H.-Y.; Jin, H.; Yang, X.-Y.; Yang, J.-S.; Qin, B. Mechanism of artemisinin phytotoxicity action: Induction of reactive oxygen species and cell death in lettuce seedlings. *Plant Physiol. Biochem.* **2015**, *88*, 53–59. [CrossRef]
36. Sirons, G.J.; Frank, R.; Sawyer, T. Residues of atrazine, cyanazine, and their phytotoxic metabolites in a clay loam soil. *J. Agric. Food Chem.* **1973**, *21*, 1016–1020. [CrossRef] [PubMed]
37. Burkhard, N.; Guth, J.A. Photolysis of organophosphorus insecticides on soil surfaces. *Pestic. Sci.* **1979**, *10*, 313–319. [CrossRef]
38. Capps, T.M.; Barringer, V.M.; Eberle, W.J.; Brown, D.R.; Sanson, D.R. Identification of a unique glucosylsulfate conjugate metabolite of profenofos in cotton. *J. Agric. Food Chem.* **1996**, *44*, 2408–2411. [CrossRef]
39. Talwar, M.P.; Ninnekar, H.Z. Biodegradation of pesticide profenofos by the free and immobilized cells of Pseudoxanthomonas suwonensis strain HNM. *J. Basic Microb.* **2015**, *55*, 1094–1103. [CrossRef] [PubMed]

40. Salunkhe, V.P.; Sawant, I.S.; Banerjee, K.; Rajguru, Y.R.; Wadkar, P.N.; Oulkar, D.P.; Naik, D.G.; Sawant, S.D. Biodegradation of profenofos by Bacillus subtilis isolated from grapevines (*Vitis vinifera*). *J. Agric. Food Chem.* **2013**, *61*, 7195–7202. [CrossRef]
41. Amalraj, A.; Suryaprabha, T.; Rajeswari, A.; Pius, A. Photocatalytic degradation of quinalphos and profenofos pesticides using UV irradiated TiO_2 nanoparticles—A kinetic study. *Mater. Focus* **2016**, *5*, 377–384. [CrossRef]
42. Lin, K.; Yuan, D.; Chen, M.; Deng, Y. Kinetics and products of photo-Fenton degradation of triazophos. *J. Agric. Food Chem.* **2004**, *52*, 7614–7620. [CrossRef]
43. Liang, B.; Yang, C.; Gong, M.; Zhao, Y.; Zhang, J.; Zhu, C.; Jiang, J.; Li, S. Adsorption and degradation of triazophos, chlorpyrifos and their main hydrolytic metabolites in paddy soil from Chaohu Lake, China. *J. Environ. Manag.* **2011**, *92*, 2229–2234. [CrossRef] [PubMed]
44. Lin, K.; Yuan, D.; Deng, Y.; Chen, M. Hydrolytic products and kinetics of triazophos in buffered and alkaline solutions with different values of pH. *J. Agric. Food Chem.* **2004**, *52*, 5404–5411.
45. Wang, L.; Zhang, L.; Chen, H.; Tian, Q.; Zhu, G. Isolation of a triazophos-degrading strain *Klebsiella* sp. E6 effectively utilizing triazophos as sole nitrogen source. *FEMS Microbiol. Lett.* **2005**, *253*, 259–265. [CrossRef]
46. Yang, C.; Li, R.; Song, Y.; Chen, K.; Li, S.; Jiang, J. Identification of the biochemical degradation pathway of triazophos and its intermediate in Diaphorobacter sp. TPD-1. *Curr. Microbiol.* **2011**, *62*, 1294–1301. [CrossRef] [PubMed]
47. Aungpradit, T.; Sutthivaiyakit, P.; Martens, D.; Sutthivaiyakit, S.; Kettrup, A.A. Photocatalytic degradation of triazophos in aqueous titanium dioxide suspension: Identification of intermediates and degradation pathways. *J. Hazard. Mater.* **2007**, *146*, 204–213. [CrossRef] [PubMed]
48. Zhu, X.; Yuan, C.; Bao, Y.; Yang, J.; Wu, Y. Photocatalytic degradation of pesticide pyridaben on TiO_2 particles. *J. Mol. Catal. A Chem.* **2005**, *229*, 95–105. [CrossRef]
49. Grisenti, R.; Schöllkopf, W.; Toennies, J.; Hegerfeldt, G.; Köhler, T.; Stoll, M. Determination of the bond length and binding energy of the helium dimer by diffraction from a transmission grating. *Phys. Rev. Lett.* **2000**, *85*, 2284. [CrossRef]
50. Saez, J.S.; Garraleta, M.H.; Anton, P.C.; Alonso, M.F. Identification of 4-bromo-2-chlorophenol as a contaminant responsible for organoleptic taint in melons. *Food Addit. Contam.* **1991**, *8*, 627–631. [CrossRef]
51. Liu, B.; McConnell, L.; Torrents, A. Hydrolysis of chlorpyrifos in natural waters of the Chesapeake Bay. *Chemosphere* **2001**, *44*, 1315–1323. [CrossRef]
52. Karkmaz, M.; Puzenat, E.; Guillard, C.; Herrmann, J. Photocatalytic degradation of the alimentary azo dye amaranth: Mineralization of the azo group to nitrogen. *Appl. Catal. B-Environ.* **2004**, *51*, 183–194. [CrossRef]